doi:10.2533/chimia.2025.52 Chimia 79 (2025) 52–59

Advancements in Nanoscale Chemical Analysis using Tip-Enhanced Raman Spectroscopy

Siiri Bienz, Chengcheng Xu, Yuanzhi Xia, Anushree Dutta, Renato Zenobi, and Naresh Kumar*

Abstract: Tip-enhanced Raman spectroscopy (TERS) has established itself as a powerful tool in nanoscale chemical analysis, providing unprecedented spatial resolution with high molecular sensitivity and chemical specificity. TERS employs localized surface plasmon resonance at the apex of a sharp scanning probe microscopy tip to overcome the diffraction limit inherent in conventional Raman spectroscopy, achieving spatial resolutions down to the nanometer scale. In this article, we highlight major advancements in TERS over the past five years from our laboratory at ETH Zurich in the following key areas: heterogeneous catalysis, photovoltaic materials, biological membranes, and on-surface molecular assembly. Our recent studies demonstrate the unique capabilities of TERS for *in situ* monitoring of catalytic reactions, nanoscale mapping of phase behavior in biomembranes, and precise characterization of photovoltaic interfaces. Through these applications, we highlight the potential of TERS for addressing critical challenges across the chemical, biological, and materials sciences. This review serves as a guide for researchers aiming to harness TERS for label-free, non-destructive nanoanalysis to advance understanding of complex molecular materials and processes through ultrahigh sensitivity, specificity, and spatial resolution.

Keywords: Biomembranes · Heterogenous catalysis · Nanoanalysis · Photovoltaic materials · Tip-enhanced Raman spectroscopy

Siiri Bienz completed her Master's degree in chemistry at ETH Zurich in 2021, where she conducted her thesis in Prof. Renato Zenobi's group, focusing on tip-enhanced optical spectroscopy for catalytic surface analysis. She began her PhD in 2022, continuing in the Zenobi Group, where her research centers on applying tip-enhanced optical spectroscopy to functional materials.

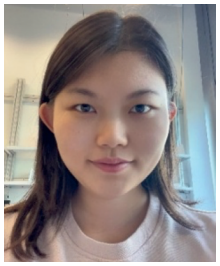

Chengcheng Xu earned her Master's degree in industrial chemistry from the Technical University of Munich in 2023. She subsequently joined the Zenobi Group at ETH Zurich as a PhD student, where her research focuses on nanoscale material analysis using TERS. Her work investigates the phase behavior of biological membranes and the mechanisms underlying various surface reactions.

Yuanzhi Xia began his PhD in surface chemistry at KU Leuven in 2017, focusing on the covalent functionalization of graphitic surfaces, using scanning probe microscopy as the primary analytical technique. After completing his PhD in chemistry in 2022, he continued as a postdoctoral researcher at KU Leuven. In 2024, he joined the Zenobi Group at ETH Zurich, where he advances his research in surface science, specializing in nanoscale analysis of chemical transformations on surfaces through scanning tunneling microscopy (STM)-based TERS.

Anushree Dutta obtained her PhD in physical chemistry from the Indian Institute of Technology Guwahati, India, in 2018. She performed her postdoctoral research at the University of Potsdam, Germany, in plasmon chemistry and single-molecule surface-enhanced Raman spectroscopy, and at the Israel Institute of Technology, Technion, focusing on sustainable energy conversion. She is currently a postdoctoral researcher in the Zenobi group at ETH Zurich, where her research centers on the nanoscale characterization of polymeric nanoparticles and catalytic reactions using TERS.

Renato Zenobi is a Professor of analytical chemistry at ETH Zurich. He is known for his pioneering work in mass spectrometry, particularly in laser-assisted and electrospray techniques, as well as near-field optical methods. After completing his MSc at ETH Zurich and PhD at Stanford, he conducted postdoctoral research in the USA and then returned to Switzerland as a Werner Fellow at EPFL. Subsequently, he joined ETH Zurich, becoming a full professor in 2000. A leading figure in tip-enhanced Raman spectroscopy, Prof. Zenobi's research continues to advance analytical methods in mass spectrometry and nanoscale analysis.

*Correspondence: Dr. N. Kumar, E-mail: naresh.kumar@org.chem.ethz.ch
Department of Chemistry and Applied Biosciences, ETH Zurich, Zurich, CH-8093, Switzerland

Naresh Kumar is a Senior Scientist and Lecturer in the Department of Chemistry and Applied Biosciences at ETH Zurich, Switzerland. His expertise is in the field of optical nanospectroscopy and nanoimaging. He earned his PhD at Utrecht University, Netherlands, focusing on the development of TERS for catalysis research. While working as a staff scientist at the National Physical Laboratory, UK, Dr. Kumar established a state-of-the-art AFM-based TERS system and applied it to tackle cutting-edge problems in heterogeneous catalysis, organic photovoltaics, polymeric materials, and nanobioimaging. Since 2020, he has led the optical nanospectroscopy and nanoimaging research in the Zenobi group at ETH Zurich.

1. What is Tip-Enhanced Raman Spectroscopy?

The demand for precise molecular-level characterization is accelerating with the advancement of nanoscience and nanotechnology, highlighting the need for analytical tools that offer nanoscale spatial resolution coupled with high sensitivity and chemical specificity. Spatial resolution of conventional optical methods such as fluorescence, infra-red (IR) and Raman spectroscopies is limited to the sub-μm (200 – 300 nm) scale due to the optical diffraction limit (λ/2NA).[1] Moreover, the sensitivity of Raman spectroscopy is notably limited due to the intrinsically weak scattering cross-sections of non-resonant molecules. Tip-enhanced optical spectroscopy (TEOS) addresses these limitations by integrating scanning probe microscopy (SPM) with optical spectroscopy techniques, enabling the acquisition of chemical and structural information at the nanometer length-scales.

Among the TEOS techniques, tip-enhanced Raman spectroscopy (TERS) and tip-enhanced photoluminescence (TEPL) spectroscopy have emerged as leading methods. In this review, we will primarily cover the recent advancements and applications of TERS. The concept of TERS was initially proposed by John Wessel in 1985.[2] Leveraging the Nobel prize winning invention of scanning tunneling microscopy (STM) at IBM Zurich,[3] TERS was first experimentally demonstrated at ETH Zurich in 2000.[4] Subsequently, three independent research groups experimentally realized TERS later that same year.[5–7]

In a TERS experiment, a silver or gold SPM tip is positioned in the focal spot of an excitation laser. When the laser frequency matches with the natural oscillation frequency of conduction electrons in the metal, a localized surface plasmon resonance (LSPR) is generated, enhancing the electromagnetic field (also called near-field) at the tip apex by several orders of magnitude. The near-field strength is further amplified by the lightning rod effect (LRE), a non-resonant enhancement arising from the sharpness of the tip.[8] Alongside electromagnetic enhancement, certain molecule-substrate interactions can also exhibit chemical enhancement (CE), further increasing the detection sensitivity of TERS. The CE mechanism in TERS arises from charge transfer between the metallic tip and the adsorbed molecule, which modifies the molecule's electronic structure and enhances its polarizability during vibrational transitions. This effect, often specific to the molecule-tip interaction, contributes an additional Raman signal enhancement factor of 10 to 10^3 beyond the electromagnetic enhancement. The combined effect of LSPR, LRE, and CE dramatically enhances both the sensitivity and spatial resolution of conventional Raman spectroscopy,[9] enabling the detection of Raman signals from even monolayers of non-resonant molecules. The spatial resolution in TERS is governed by the size and geometry of the metallic nanostructure at the tip apex, allowing near-field confinement to regions as small as a few nanometers. Under ultrahigh-vacuum (UHV) and cryogenic conditions, TERS has achieved spatial resolutions approaching the Angstrom scale, enabling single-molecule imaging.[10,11] These controlled conditions stabilize the tip and minimize both instrumental and molecular drift, which is ideal for high-resolution applications. Under ambient conditions, TERS has been extensively used for nanoscale chemical characterization across the physical, chemical, materials, and biological sciences, showcasing its suitability for real-world samples and practical environments.

TERS can be implemented with both atomic force microscopy (AFM) and STM, each offering unique strengths. STM-TERS is particularly advantageous for conductive samples, such as molecular monolayers on metallic substrates, and generally provides higher enhancement and better spatial resolution than AFM-TERS. However, the requirement for electron tunneling restricts STM-TERS primarily to the study of molecular monolayers or single-layer/2D materials. In contrast, AFM-TERS is compatible with a wider variety of materials, including insulating samples.

TERS can be performed in different optical geometries, including top-, bottom-, side- and parabolic-illumination, each with distinct advantages.[12–15] Bottom-illumination directs the laser through a transparent substrate onto the sample using a high numerical aperture (NA) objective lens, often with radially polarized light to achieve strong z-polarization in the focal spot.[16] Side-illumination is ideal for opaque samples, directing the laser from the side towards the tip-sample interface, typically with linearly polarized light. Top-illumination requires the probe to be angled relative to the sample and uses linearly polarized light. Although parabolic illumination can be challenging to align, it provides a balanced alternative to top and bottom configurations, offering a high NA while avoiding chromatic aberration. The choice of illumination geometry depends on the specific properties of the sample and the requirements of the experiment (Fig. 1).

In this review, we highlight recent advancements from our laboratory at ETH Zurich over the past five years in the application of TERS to four key areas: (i) heterogeneous catalysis, (ii) photovoltaic materials, (iii) biological membranes, and (iv) on-surface molecular assembly. Alongside our own research contributions at ETH Zurich, we also emphasize significant recent TERS studies from other research groups in these areas.

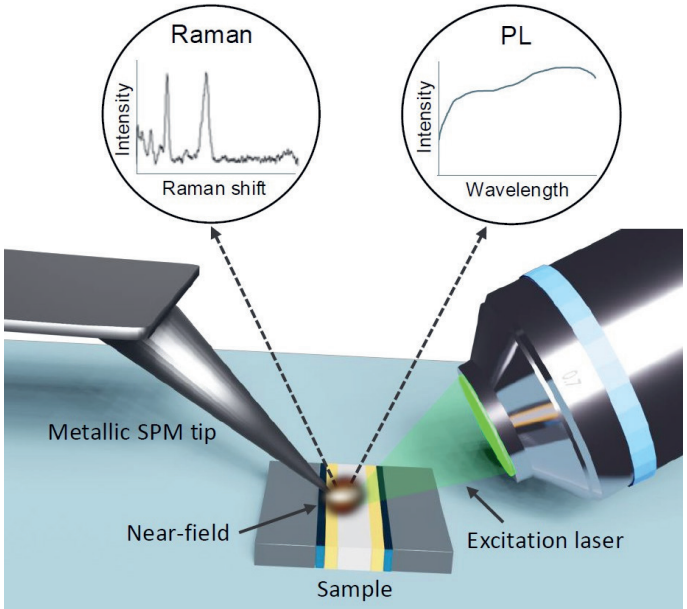

Fig. 1. Schematic illustration of a side-illumination TERS set-up. The combination of LSPR and LRE generates a highly intense and localized near-field at the apex of a metallic SPM tip. Raman and photoluminescence signals from the molecules present in the near-field are enhanced by several orders of magnitude enabling hyperspectral TERS and TEPL imaging at the nanoscale.

2. Advances in Nanoscale Chemical Analysis Using TERS

2.1 *Heterogenous Catalysis*

Heterogeneous catalysis is essential to a wide range of chemical and energy conversion processes in industry.[17–19] Addressing global sustainability challenges requires not only the development of new catalytic materials with improved activity and selectivity, but also advanced analytical techniques to monitor and understand catalytic processes at the nanoscale. These processes often involve structural changes in the catalyst during operation, such as the generation of active species, the adsorption and desorption of reactants, products, and intermediates, and site-specific reactions.[9,19,20] TERS has emerged as a powerful nanoanalytical tool for characterizing these catalytic phenomena, offering unique insights into surface chemistry and dynamics at the nanoscale.[21]

Visualizing catalytically active sites: TERS has proven valuable in investigating how catalyst nanostructure influences efficiency. The Kurouski group used TERS mapping to demonstrate the enhanced catalytic efficiency of the Suzuki-Miyaura reaction on the edges of Au@Pd microplates, as compared to the relatively inert flat terraces.[22] In a related study, they also observed a higher rate of 4-nitrothiophenol (4-NTP) reduction to *p,p'*-dimercaptoazobisbenzene (DMAB) and 4-aminothiophenol (4-ATP) at the edges of Au@Pd microplates, discovering the spatially selective catalytic activity of these regions.[23] Our group used ambient TERS to investigate the 'hydrogen spill-over effect' *via* selective hydrogenation of chloronitrobenzenethiol (CNBT) to chloroaminobenzenethiol (CABT) on a Pd-submonolayer/Au(111) bimetallic catalyst surface.[24] The hydrogen spill-over effect in the hydrogenation reaction on Pd/Au substrates refers to the migration of dissociated H atoms from the Pd surface, where H_2 dissociation occurs, to the neighboring Au surface. High-resolution TERS imaging confirmed hydrogen spill-over through the presence of CABT molecules on the Au(111) surface within 20 nm distance from the Pd/Au boundary, an otherwise inactive region for CNBT-to-CABT hydrogenation. The Ren group employed electrochemical TERS (EC-TERS) to observe the geometric and electronic restructuring of active sites in MoS_2 flakes during the hydrogen evolution reaction. TERS measurements revealed that the edges of MoS_2 flakes undergo a synergistic reconstruction toward the basal plane, reducing the activation energy barrier and facilitating the electrocatalytic reaction.[11]

Determining structure-activity relationships: TERS is uniquely suited for elucidating structure-activity relationships in catalytic processes at the molecular level. For instance, Sun *et al.* investigated the impact of adsorbate orientation on plasmon-driven coupling reactions, such as the conversion of 4-ATP and 4-NTP to DMAB on Au(111) and Ag(111) surfaces.[25] Their findings revealed that the oxidative coupling of 4-ATP occurred on Au(111) under 632.8 nm laser irradiation, while the reductive coupling of 4-NTP required a 532 nm laser. In contrast, neither wavelength induced the coupling reactions on Ag(111), which was attributed to the vertical orientation of the adsorbed molecules on this surface. In a recent study, our group combined high-resolution TERS imaging, molecular-resolution STM imaging, and density functional theory (DFT) modeling to investigate the role of molecular arrangement in the photocatalytic coupling of 4-NTP to DMAB on Au surfaces. We observed that the coupling efficiency was significantly lower in a densely-packed 4-NTP adlayer on the Au(111) surface compared to a disordered adlayer as shown in Fig. 2. DFT calculations confirmed that a combination of steric hindrance and high energy barrier in the closed-packed 4-NTP adlayer resulted in reduced coupling efficiency, revealing a clear structure-activity relationship.[26]

Chen *et al.* employed EC-TERS for *operando* characterization of the structure-activity relationship of iron(II) phthalocyanine (FePc) during the oxygen reduction reaction at the nanoscale.[27] They observed a reversible change in the Raman spectrum of FePc, which was attributed to the nonplanar geometry of FePc during catalysis. This reversible behavior was accompanied by irreversible degradation of FePc, which proceeded *via* direct loss of Fe^{2+}, unveiled through time-resolved EC-TERS measurements.

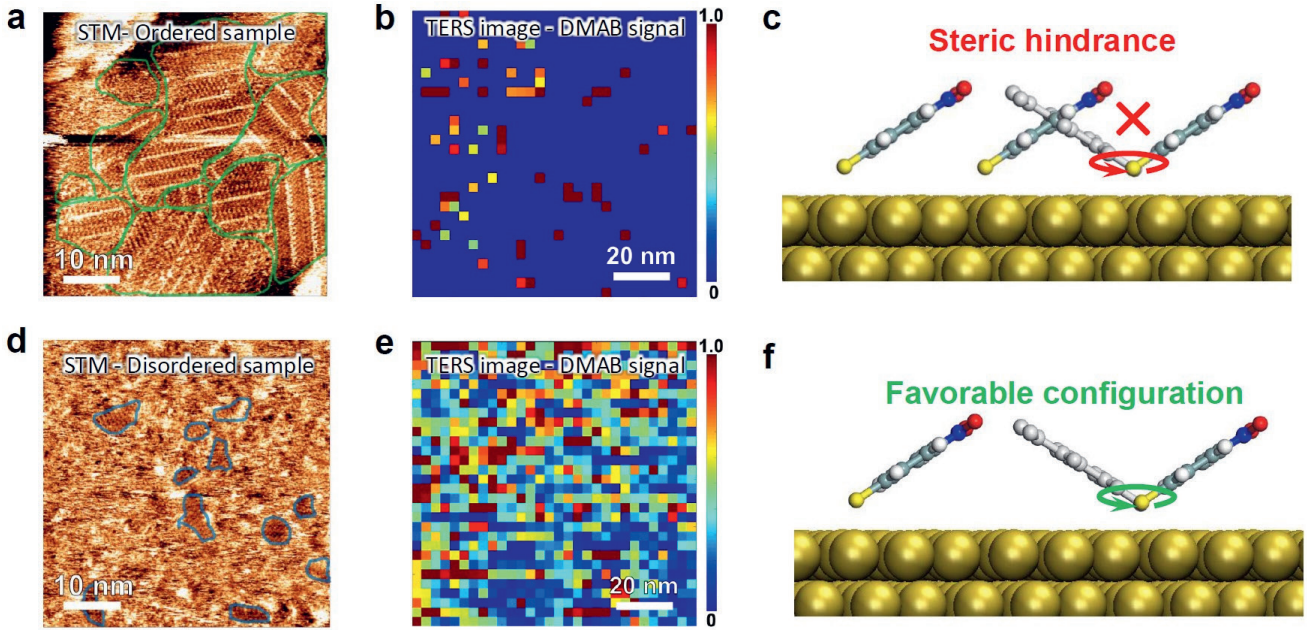

Fig. 2. (a) Molecular-resolution STM image and (b) TERS image of the DMAB signal measured on an ordered 4-NTP-functionalized Au(111) sample. (c) DFT calculations indicate that in the close-packed arrangement shown in Panel a, 4-NTP molecules cannot adopt a vertical orientation due to a high energy barrier. Instead, rotation around the vertical axis is energetically favorable, but it prevents NO_2 groups of adjacent molecules from coming into contact, explaining the low efficiency of photocatalytic dimerization to DMAB observed in Panel b. (d) Molecular-resolution STM image and (e) TERS image of the DMAB signal measured on a disordered 4-NTP-functionalized Au(111) sample. (f) In the disordered arrangement, the random orientation of 4-NTP allows NO_2 moieties to approach each other upon rotation, resulting in significantly enhanced DMAB formation, as shown in Panel e. Reproduced with permission from ref. [26] Copyright 2022 American Chemical Society.

Detecting catalytic reaction products: TERS enables detection of reaction products with high sensitivity and specificity, which may remain undetected in bulk or ensemble measurements. For example, Wang *et al.* observed the formation of 4-NTP thiolate during TERS analysis of a 4-NTP adlayer on Au nanoplates.[28] Calculations using DFT and finite element methods indicated that this transformation likely results from hot electrons generated *via* LSPR, rather than thermal desorption. El-Khoury's group used hyperspectral TERS imaging in an aqueous environment to identify both *cis*-DMAB and *trans*-DMAB as products of 4-NTP photocatalytic dimerization on Au nanoplates.[29] Their study showed that the reaction was confined to distinct hotspots on the substrate, suggesting that molecular crowding and steric effects played a critical role in the dimerization process. Tip-enhanced fluorescence (TEFL) imaging is also an effective tool to study real-life catalysts. For instance, our group employed hyperspectral TEFL imaging to investigate the deactivation of zeolite ZSM-5 catalysts during the methanol-to-hydrocarbon (MTH) reaction.[30] TEFL imaging revealed a higher amount of coke formation at the crystal steps of the ZSM-5 catalyst surface, indicating that these topographic features exhibit faster deactivation during the MTH reaction.

Understanding catalytic processes on Au surfaces: TERS has also been instrumental in understanding complex catalytic processes on Au surfaces like electrochemical oxidation and spill-over effects. Pfisterer *et al*. observed the formation of Au_2O_3 and Au_2O species during electrochemical oxidation on Au(111) electrodes by *operando* EC-TERS.[31] In another study, Su *et al*. used EC-TERS to monitor the generation and diffusion of hydroxyl (OH) radicals on Pd/Au(111) bimetallic surfaces in the presence of H_2O_2.[32] They found that the Pd surface, especially at step edges, exhibited higher activity for OH radical generation, while Au remained inert to oxidation. Further TERS imaging revealed that OH radicals generated on Pd step edges could diffuse to Au sites, initiating oxidative reactions with a diffusion length of approximately 5.4 nm, providing valuable insight into the catalytic spill-over.

We employed TERS to elucidate the mechanism of oxygen activation on an Au(111) surface.[33] Using the oxidation of 4-ATP to 4-NTP as a model reaction, we demonstrated for the first time that oxidation can indeed proceed on a bulk Au(111) surface. By treating a 4-ATP-functionalized Au(111) sample with isotopically labeled water ($H_2{}^{18}O$), we provided the first empirical evidence that molecular oxygen activation on bulk Au(111) occurs through a water-mediated mechanism.

Inducing and monitoring photocatalytic polymerization using TERS: TERS has shown significant potential to monitor plasmon-catalyzed polymerization at the nanoscale. Sometime ago, Zhang *et al*. demonstrated plasmon-induced coupling of dibenzo(1,2)dithiine-3,8-diamine (D3ATP), with the plasmonic TERS tip inducing coupling reactions at specific locations on an Au(111) surface.[34] More recently, our group used TERS imaging to simultaneously induce and monitor plasmon-induced [4+4]-cycloaddition polymerization within anthracene-based monomer monolayers on Au(111). TERS imaging with a spatial resolution of 3.7 nm provided direct evidence of covalent bond formation.[35] These studies illustrate the potential of TERS in nanolithography and the creation of ultrathin polymer films with defined structural dimensions.

These studies showcase the remarkable ability of TERS to reveal detailed nanoscale insights into heterogeneous catalytic processes, enabling a better understanding of catalytic efficiency, reaction intermediates, structure-activity relationships, and catalytic spill-over effects. Through precise and high-resolution measurements, TERS offers a powerful toolset for advancing catalytic science at the molecular level.

2.2 Photovoltaic Materials

Thin-film optoelectronic devices based on photovoltaic materials are a rapidly advancing field. While confocal Raman spectroscopy is widely used for characterizing photovoltaic materials, its spatial resolution is inadequate for investigating nanoscale features critical to device performance, such as defects, charge carrier recombination, and interlayer diffusion. With its superior spatial resolution, TERS is an effective tool for the nanoscale analysis of photovoltaic materials.

Early applications of TEOS to photovoltaic materials: the Meixner group was among the first to demonstrate the application of TERS and TEPL to analyze photovoltaic materials. They investigated local changes in poly(3-hexylthiophene) (P3HT): [6,6]-phenyl-C_{61}-butyric acid methyl ester (PCBM) blends subjected to different annealing times.[36] Correlative topographical and TEOS imaging on the 30-minute annealed sample revealed that PCBM molecules tend to aggregate at higher topography points. Using the full width at half maximum of the P3HT C=C stretching Raman peak, they demonstrated that this PCBM clustering reduced crystallinity within P3HT domains. On the other hand, TEOS measurements of the 5-minute annealed sample, which appeared homogeneous in confocal Raman and photoluminescence measurements, revealed ellipsoidal islands smaller than those in the 30-minute sample, confirming the exciton diffusion length in P3HT of 9 nm.

We employed TERS and TEPL imaging to investigate operational organic solar cells with an active layer composed of a blend of a polymer called poly[(2,1,3-benzothiadiazole-4,7-diyl)-*alt*-(4,9-dihydro-4,4,9,9-tetraoctylbenzo[1′′,2′′:4,5;4′′,5′′:4′,5′] bissilolo[3,2-b:3′,2′-b′]dithiophene-2,7-diyl)] (C8SiIDT-BT) and a fullerene derivative called 1′,4′-dihydro-naphtho[2′,3′:1,2][5,6] fullerene-C_{60} (ICMA).[37] By combining TERS with photoconductive AFM (PC-AFM), we simultaneously measured topographical, electrical, and optical images of the C8SiIDT-BT active layer, achieving spatial resolution below 20 nm as shown in Figs. 3a-e. High-resolution TERS and TEPL images distinguished surface and subsurface structures, enabling the reconstruction of the blend morphology within a 10 nm depth from the surface. Our findings, corroborated by photocurrent measurements, revealed the optimal polymer-to-fullerene ratio crucial for maximizing photocurrent generation in C8SiIDT-BT:ICMA solar cells. This study underscored the importance of blend morphology in enhancing photoconversion efficiency in organic photovoltaic devices.

Nanoscale investigation of Sb_2Se_3-based thin-film solar cells: We recently applied TERS to investigate Sb_2Se_3-based thin-film solar cells, a second-generation photovoltaic technology.[38] These cells consist of multiple layers that are only a few hundred nanometer thick. The absorber-buffer interface plays a pivotal role in charge carrier transport, recombination losses, and defect formation. We employed TERS to investigate an Sb_2Se_3-based thin-film solar cell comprising a CdS buffer layer and a ZnO conductive layer, focusing specifically on the absorber-buffer interface (Fig. 3f). TERS measurements revealed that the interface between the Sb_2Se_3 and CdS layers was not sharply defined. Instead, significant chemical intermixing was detected between these layers, as identified by their characteristic Raman marker bands. This intermixing resulted in a thicker-than-expected interface of 295 ± 70 nm thickness, most likely due to pore formation during the CdS chemical bath deposition process. Additionally, TERS analysis revealed the undesired penetration of CdS into the Sb_2Se_3 layer with a spatial resolution of 10 nm as shown in Figs. 3g–j, which can potentially reduce power conversion efficiency. TERS imaging also detected ZnO, used as the conductive layer, in the Sb_2Se_3-rich region, co-localized with CdS. This finding suggests that the ZnO deposition process *via* radio frequency magnetron sputtering, a high-energy method, led to excessive ZnO penetration, which can potentially compromise device performance. This is particularly

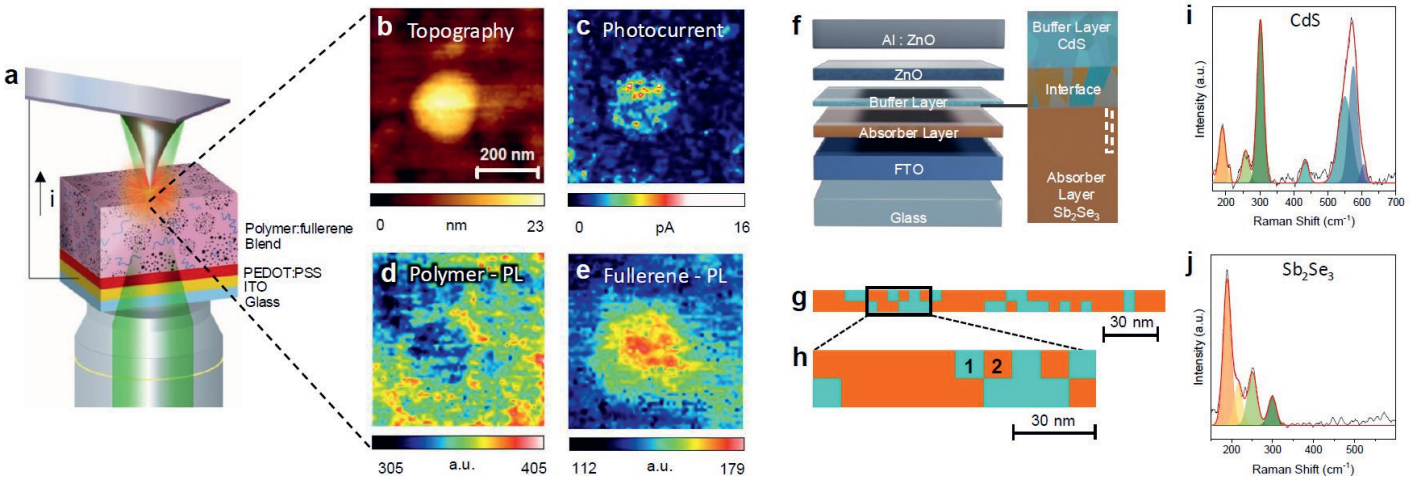

Fig. 3. (a) Schematic illustration of the experimental setup used to perform *in situ* topographical, chemical and electrical imaging of the operational C8SiIDT-BT(polymer):ICMA (fullerene) organic solar cell. Simultaneously recorded (b) topography (c) photocurrent (d) polymer PL and (e) fullerene PL images of the solar-cell active layer. Panels a-e are reproduced from ref. [37] with permission from The Royal Society of Chemistry. (f) Schematic illustration of the multilayered Sb_2Se_3-based thin-film solar cell. (g, h) Overlay image of the TERS maps of the Sb_2Se_3 (190 cm^{-1}, orange) and CdS (300 cm^{-1}, blue) Raman signals. Step size: 10 nm. (i, j) TERS spectra measured at the locations marked as 1 (CdS) and 2 (Sb_2Se_3) in Panel h. Panels g-j are reproduced with permission from ref. [38] Copyright 2024 American Chemical Society.

significant as heterojunctions - where the n-type ZnO layer is separated from the p-type Sb_2Se_3 layer by a CdS buffer - are known to achieve high efficiency when these layers remain distinct.

The application of TERS and TEPL imaging for nanoscale characterization of photovoltaic materials offers a promising path for advancing this field. TEOS is especially powerful when integrated with other SPM methods such as conductive-AFM (C-AFM) and Kelvin probe force microscopy, offering simultaneous topographical, chemical, and electrical imaging at the nanoscale. Such *in situ* multiparameter imaging can provide comprehensive insights into the nanoscale properties of photovoltaic materials, accelerating ongoing efforts to optimize their efficiency and stability.

2.3 *Biomembranes*

Biological membranes are highly dynamic and complex structures essential for maintaining cellular integrity, signaling, transport, and environmental interactions.[39–41] Biomimetic membranes, as simplified models, are valuable for studying fundamental membrane properties under controlled conditions.[42] Due to its non-destructive and label-free nature, TERS is an ideal nanoscale imaging technique for investigating both biological and biomimetic membranes, offering high-resolution insights into lipid phase separation, lipid packing, molecular organization, and overall chemical complexity.[43]

Supported lipid monolayers: Supported lipid membranes are valuable models for studying the properties of biomembranes. We applied hyperspectral TERS imaging to investigate nanoscale heterogeneities,[44] phase segregation,[45] molecular ordering,[46] and lipid distribution[47] in biomimetic lipid membranes prepared using the Langmuir-Blodgett (LB) technique. For instance, we demonstrated the first correlative topographical and hyperspectral TERS imaging of dipalmitoylphosphatidylcholine (DPPC) monolayers on an Au surface as shown in Figs. 4a and b.[46] High-resolution TERS images revealed nanoscale discontinuities/holes within the transferred DPPC monolayer. Additionally, by performing ratiometric analysis of the 2850 and 2930 cm^{-1} Raman bands (I_{2930}/I_{2850}) in the C-H stretching region (Fig. 4b), we successfully mapped the molecular packing in the DPPC monolayer, distinguishing areas of high and low disorder. In a related study, we utilized TERS imaging to examine phase separation in d_{62}-DPPC: 1,2-dioleoyl-sn-glycero-3-phosphocholine (DOPC) (1:1) binary lipid monolayers.[44] By utilizing C-H and C-D stretching Raman signals, we visualized distinct lipid domains, identifying d_{62}-DPPC-rich and DOPC-rich regions. Interestingly, instead of a complete segregation, partial phase separation was observed. Using multivariate analysis of the TERS data, a transition region of 40 - 120 nm was identified between the phase separated domains. This finding suggests a smooth transition between phase-separated regions of binary lipid systems rather than an abrupt boundary, providing a deeper understanding of phase behavior at the nanoscale.

In a more recent study, we examined the effect of subtle structural modifications on phase separation in binary lipid membranes.[48] TERS imaging of d_{62}-DPPC:DPPC (1:1) monolayers on an Au surface, transferred using the LB method, revealed partial phase separation (Figs. 4c and d), similar to our previous study of d_{62}-DPPC:DOPC (1:1) monolayers. Furthermore, the study identified molecular conformation and polarity as key factors driving the phase separation of deuterated and non-deuterated lipids in the d_{62}-DPPC:DPPC monolayer.

Supported lipid bilayers: TERS can also be a powerful tool for nanoanalysis of supported lipid bilayers, achieving submolecular resolution in the vertical dimension. Our TERS investigation of DPPC bilayers supported on glass revealed a uniquely shaped C-H stretching band, distinct from that observed in far-field Raman measurements.[50] Through spectral deconvolution and supporting DFT calculations we showed that this unique TERS signal primarily originated from the CH_3 groups within the choline headgroup (size < 1 nm) of the DPPC molecules. These findings underscore the ultrahigh sensitivity of TERS for label-free analysis of lipid membranes under ambient conditions.

Biological membranes: While supported lipid monolayers and bilayers have provided novel insights, direct nanoscale imaging of biological membranes remains a challenging research frontier. Biological membranes, composed of lipids, proteins, and other macromolecules facilitate cell communication by regulating molecular transport.[51] Although single-point TERS measurements have been employed in biomembrane studies, TERS imaging of biological membranes is still being developed. For instance, we imaged newly-synthesized phospholipids through deuterium labelling in mouse preadipocyte cells using TERS.[52] On the other hand, Alexander and Schultz used antibody-conjugated nanoparticles to map membrane proteins in biological membranes by TERS imaging.[53] However, these studies relied on labeling, which may compromise the functional integrity of biomolecules.[54]

Recent advancements in TERS have enabled the label-free capture of nanoscale heterogeneity in cell membranes. Using TERS imaging, intricate details of membrane composition and

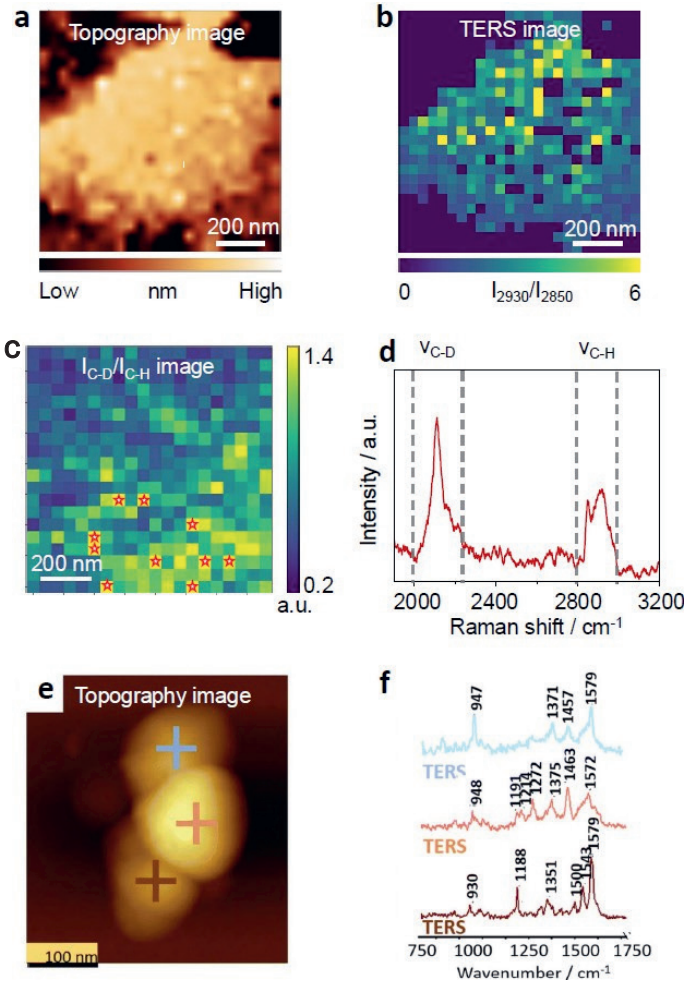

Fig. 4. Correlative (a) STM topography image and (b) TERS image of the I_{2930}/I_{2850} ratio measured from a DPPC monolayer/Au (111) sample. Integration time: 2 s. Step size: 40 nm. TERS image reveals nanoscale heterogeneities including holes in the DPPC monolayer that are invisible in the topography image. Furthermore, areas of high (yellow) and low (blue) disorder are mapped with a nanoscale resolution. Panels a and b are reproduced with permission from ref. [46] (c) TERS image of the $I_{C\text{-}D}/I_{C\text{-}H}$ ratio highlighting the phase separated d_{62}-DPPC-rich domain in a d_{62}-DPPC:DPPC (1:1) monolayer. (d) Plot showing the average of the 10 TERS spectra measured at the positions marked in Panel c confirming the higher intensity of the C-D signal in the d_{62}-DPPC-rich region. Panels c and d are reproduced with permission from ref. [48] Copyright 2024 American Chemical Society. (e) AFM topography image of REVs. (f) TERS spectra measured from the REVs at the locations marked in Panel e. Panels e and f are reproduced from ref. [49] with permission from The Royal Society of Chemistry.

organization have been revealed in the plasma membranes of human dermal keratinocytes[55] and colon cancer cells.[56] In our laboratory, we applied label-free TERS to study human pancreatic cancer cells, identifying distinct domains rich in phenylalanine and histidine, as well as regions enriched in phosphatidylcholine lipids, proteins, and cholesterol.[47] These findings reveal the nanoscale heterogeneity of cell membranes with aggregation of biomolecules into distinct nanoscopic regions.

TERS has also been applied to study cell-derived membranes such as red blood cell extracellular vesicles (REVs) shown in Fig. 4e. Stepanenko *et al.* used TERS to capture distinct protein and lipid compositions in REV microvesicles.[49] The TERS spectra in Fig. 4f, measured at the locations marked in Fig. 4e, display pronounced amide II bands representing protein secondary structures including β-sheets and α-helices, with contributions from amino acid residues such as tryptophan and histidine. Additionally, vibrations in the 1350–1380 cm^{-1} and 1272 cm^{-1} ranges show the presence of lipids such as phosphatidylethanolamine, phosphatidylcholine and cholesterol. These results demonstrate the unique ability of TERS to non-destructively capture membrane heterogeneity in extracellular vesicles.

2.4 *On-Surface Molecular Assembly*

The design of on-surface molecular assemblies with targeted chemical composition, spatial orientation, and intermolecular interactions, is essential for controlling surface properties in fields such as catalysis, materials science, and nanotechnology.[57,58] Molecular arrangements on atomically flat surfaces are strongly influenced by the underlying substrate. Since its invention, STM has become an invaluable tool for visualizing on-surface molecular assemblies with atomic-scale resolution.[59–61] For example, the De Feyter group used STM to directly visualize molecular self-assembly dynamics under various nanoconfinement conditions, providing insights into the evolution of novel molecular architectures.[60,62,63]

TERS expands the capabilities of STM by adding chemical specificity at the single-molecule level. A pioneering study by the Dong group demonstrated the potential of TERS with single-molecule imaging at an unprecedented spatial resolution of approximately 0.5 nm under ultrahigh vacuum and cryogenic conditions.[64] This breakthrough underscored the capability of TERS for sub-nanometer chemical imaging, enabling a clear distinction between two adjacent molecules in van der Waals contact (a metal-centered porphyrin, and a free-base porphyrin), despite minimal structural differences. Due to the surface selection rules, TERS spectra are highly sensitive to adsorption configurations and orientations, allowing precise determination of molecular geometry and orientation. By correlating TERS spectra of individual molecules at distinct adsorption sites with DFT calculations, it is possible to resolve their structural and chemical characteristics with high precision.

We applied TERS to investigate the molecular orientation and spatial distribution of on-surface coordination complexes under ambient conditions. In this study, a self-assembled monolayer of 4-mercaptopyridine (4-PySH) anchored to an Au(111) surface served as a buffer layer for coordinating cobalt tetraphenylporphyrin (CoTPP) molecules, as illustrated in Fig. 5a.[65] Our results demonstrated that the 4-PySH buffer layer effectively coordinated with the CoTPP molecules, enhancing the visibility of characteristic porphyrin peaks in the TERS spectra. This enhancement occurred because the buffer layer weakened the CoTPP-Au(111) surface interaction. Furthermore, high-resolution TERS imaging of CoTPP/4-PySH on Au(111) revealed three distinct spectra (Fig. 5b) indicating different orientations of the CoTPP/4-PySH coordination species. By correlating experimental results with DFT simulations, the TERS spectra could be successfully assigned to specific molecular orientations.

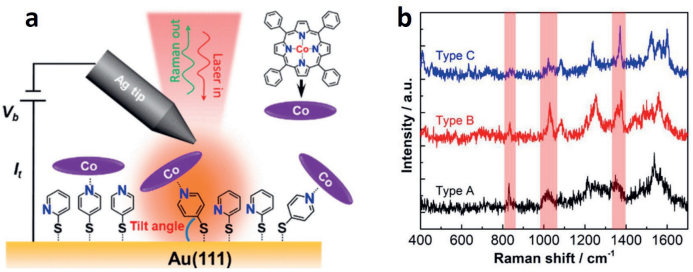

Fig. 5. (a) Schematic diagram of the TERS setup used to examine CoTPP-4PySH coordination complex on an Au surface. (b) Three types of TERS spectra observed in TERS imaging. The spectra display different intensities of the bands marked by red stripes, indicating three distinct orientations of the CoTPP-4PySH complex on the Au surface. Reproduced with permission from ref. [65] Copyright 2021 American Chemical Society

In another study, we applied hyperspectral TERS imaging to visualize the decomposition process of a 4-PySH self-assembled monolayer on an Au(111) surface under ambient conditions.[66] With 5 nm spatial resolution, TERS enabled the spectroscopic detection of reactive intermediates involved in the degradation process, which were verified using DFT simulations. This study highlighted the potential of TERS for quantitative analysis of on-surface decomposition chemistry at the nanoscale.

3. Conclusions and Outlook

Over the past two decades, TERS has established itself as a powerful tool for nanoscale chemical analysis, offering single-molecule sensitivity, chemical specificity, and in some cases even sub-molecular spatial resolution. Despite its remarkable capabilities, widespread adoption of TERS remains hindered by several practical challenges. A key limitation lies in the preparation of high-performance TERS tips, which are critical for achieving strong plasmonic enhancement. While the fabrication of electrochemically etched STM-TERS tips is relatively straightforward, the preparation of metal-coated AFM-TERS tips requires meticulous attention to detail. Specifically, the cleanliness of the physical vapor deposition chamber, the use of high-purity (≥99.99%) Ag or Au materials, and thorough cleaning of AFM cantilevers, such as using UV-ozone treatment prior to metal coating, are essential to achieve a high yield of plasmonically active TERS tips.

Another critical factor influencing the success of TERS measurements is the power of the excitation laser. Excessive laser power can damage the metal coating on the TERS tip, alter the tip apex geometry due to plasmonic heating, or cause thermal degradation of the sample. To mitigate these risks, maintaining a low laser power, typically around 100 μW, is recommended to preserve both the integrity of the TERS tip and the sample during measurements.

A common misconception in TERS is that the near-field enhancement must always yield a Raman signal contrast several orders of magnitude higher than the far-field signal, as often seen in surface-enhanced Raman spectroscopy. However, this ultrahigh contrast is typically observed only in 'gap mode' TERS, where the sample is positioned between the TERS tip and a metallic substrate. In 'non-gap mode' TERS, where a dielectric substrate is used, the contrast is often much lower, sometimes only by a factor of 1 or 2. Nevertheless, since the plasmonic enhancement is confined to the nanoscopic volume at the tip apex, even a modest contrast is sufficient to achieve the nanoscale spatial resolution that defines TERS.

As highlighted in this review, TERS has proven to be particularly valuable in heterogeneous catalysis, providing novel nanoscale insights into active sites, reaction intermediates, and structure-activity relationships. Looking ahead, we envisage that TERS will be increasingly employed *in operando* settings, enabling the dynamic monitoring of catalytic processes under industrially relevant conditions, and offering novel insights into catalytic mechanisms. In thin-film photovoltaic devices, TERS has provided crucial insights into chemical composition, nanoscale defects, photocurrent generation and interlayer diffusion. By enabling high-resolution imaging of phase separation and molecular interactions, TERS holds significant potential to accelerate the development of efficient organic and inorganic solar cells. Expanding TERS applications to emerging materials, such as perovskites and tandem solar cells, could uncover previously inaccessible details about their nanoscale interfaces and dynamic processes.

For biomimetic and biological membranes, TERS has contributed significantly to understanding lipid organization, molecular heterogeneity, and phase separation, without fluorescent labelling. Its ability to probe supported bilayer lipid membranes with sub-nanometer axial resolution under ambient conditions underscores its ultrahigh sensitivity for studying cellular biology. Future TERS applications could focus on more complex biological systems, such as investigating membrane-protein interactions, drug-membrane dynamics, or lipid rafts, offering deeper understanding of these fundamental cellular processes. In self-assembled molecular systems, TERS has proven highly effective in resolving molecular arrangements, orientations, and chemical interactions. As discussed in this article, combining TERS with advanced computational techniques, such as DFT, enables detailed analysis of complex molecular processes such as photocatalytic reactions and decomposition chemistry. Expanding TERS applications to *in situ* monitoring of dynamic molecular systems could further advance our understanding of on-surface molecular assemblies.

The unique capability of TERS for nanoscale chemical imaging with ultrahigh sensitivity and chemical specificity holds significant potential to drive innovations across diverse research areas in the physical, chemical, material, and biological sciences. We anticipate that integrating TERS with complementary techniques, such as high-speed or electrical-mode AFM, electrochemical analysis, or nano-IR spectroscopy, will further expand its applications, providing deeper insights into complex molecular systems.

Author Contributions

All authors contributed equally to the scientific discussions and writing of this manuscript. NK acknowledges financial support from Sichuan Province Science and Technology Project (2024YFHZ0288).

Received: November 24, 2024

[1] E. Abbe, *Arch. Mikrosk. Anat*. **1873**, *9*, 413 https://doi.org/10.1007/bf02956173.
[2] J. Wessel, *J. Opt. Soc. Am. B* **1985**, *2*, 1538, https://doi.org/10.1364/josab.2.001538.
[3] G. Binnig, H. Rohrer, *Angew. Chem. Int. Ed.* **1987**, *26*, 606, https://doi.org/10.1002/anie.198706061.
[4] R. M. Stöckle, Y. D. Suh, V. Deckert, R. Zenobi, *Chem. Phys. Lett*. **2000**, *318*, 131, https://doi.org/10.1016/S0009-2614(99)01451-7.
[5] M. S. Anderson, *Appl. Phys. Lett*. **2000**, *76*, 3130, https://doi.org/10.1063/1.126546.
[6] N. Hayazawa, Y. Inouye, Z. Sekkat, S. Kawata, *Opt. Commun*. **2000**, *183*, 333, https://doi.org/10.1016/S0030-4018(00)00894-4.
[7] B. Pettinger, G. Picardi, R. Schuster, G. Ertl, *Electrochemistry* **2000**, *68*, 942, https://doi.org/10.5796/electrochemistry.68.942.
[8] M. Asghari-Khiavi, B. R. Wood, P. Hojati-Talemi, A. Downes, D. McNaughton, A. Mechler, *J. Raman Spectrosc*. **2012**, *43*, 173, https://doi.org/10.1002/jrs.3021.
[9] N. Kumar, S. Mignuzzi, W. Su, D. Roy, *EPJ Techn. Instrum*. **2015**, *2*, 9, https://doi.org/10.1140/epjti/s40485-015-0019-5.
[10] Y. Zhang, B. Yang, A. Ghafoor, Y. Zhang, Y.-F. Zhang, R.-P. Wang, J.-L. Yang, Y. Luo, Z.-C. Dong, J. G. Hou, *Natl. Sci. Rev.* **2019**, *6*, 1169, https://doi.org/10.1093/nsr/nwz180.
[11] T.-X. Huang, X. Cong, S.-S. Wu, J.-B. Wu, Y.-F. Bao, M.-F. Cao, L. Wu, M.-L. Lin, X. Wang, P.-H. Tan, B. Ren, *Nat. Catal.* **2024**, *7*, 646, https://doi.org/10.1038/s41929-024-01148-x.
[12] Z. Yang, J. Aizpurua, H. Xu, *J. Raman Spectrosc*. **2009**, *40*, 1343, https://doi.org/10.1002/jrs.2429.
[13] D. Mehtani, N. Lee, R. D. Hartschuh, A. Kisliuk, M. D. Foster, A. P. Sokolov, J. F. Maguire, *J. Raman Spectrosc*. **2005**, *36*, 1068, https://doi.org/10.1002/jrs.1409.
[14] T. Deckert-Gaudig, M. Richter, D. Knebel, T. Jähnke, T. Jankowski, E. Stock, V. Deckert, *Appl. Spectrosc*. **2014**, *68*, 916, https://doi.org/10.1366/13-07419.
[15] X. Wang, S.-C. Huang, T.-X. Huang, H.-S. Su, J.-H. Zhong, Z.-C. Zeng, M.-H. Li, B. Ren, *Chem. Soc. Rev*. **2017**, *46*, 4020, https://doi.org/10.1039/C7CS00206H.
[16] N. Kumar, B. M. Weckhuysen, A. J. Wain, A. J. Pollard, *Nat. Protoc*. **2019**, *14*, 1169, https://doi.org/10.1038/s41596-019-0132-z.
[17] X. Liu, H.-J. Peng, *Engineering* **2024**, *39*, 25, https://doi.org/10.1016/j.eng.2023.07.021.
[18] S. Mitchell, R. Qin, N. Zheng, J. Pérez-Ramírez, *Nat. Nanotechnol*. **2021**, *16*, 129, https://doi.org/10.1038/s41565-020-00799-8.
[19] J.-L. Yang, Y.-W. Zhou, M.-Y. Jia, Q. Liu, Z.-F. Cai, *ChemCatChem* **2024**, *16*, e202400370, https://doi.org/10.1002/cctc.202400370.

[20] P. Pienpinijtham, Y. Kitahama, Y. Ozaki, *Nanoscale* **2022**, *14*, 5265, https://doi.org/10.1039/D2NR00274D.
[21] D. Mrđenović, Z.-F. Cai, Y. Pandey, G. Luca Bartolomeo, R. Zenobi, N. Kumar, *Nanoscale* **2023**, *15*, 963, https://doi.org/10.1039/D2NR05127C.
[22] Z. Li, R. Wang, D. Kurouski, *J. Phys. Chem. Lett*. **2020**, *11*, 5531, https://doi.org/10.1021/acs.jpclett.0c01631.
[23] Z. Li, D. Kurouski, *J. Phys. Chem. C* **2020**, *124*, 12850, https://doi.org/10.1021/acs.jpcc.0c04274.
[24] H. Yin, L.-Q. Zheng, W. Fang, Y.-H. Lai, N. Porenta, G. Goubert, H. Zhang, H.-S. Su, B. Ren, J. O. Richardson, J.-F. Li, R. Zenobi, *Nat. Catal*. **2020**, *3*, 834, https://doi.org/10.1038/s41929-020-00511-y.
[25] J.-J. Sun, H.-S. Su, H.-L. Yue, S.-C. Huang, T.-X. Huang, S. Hu, M. M. Sartin, J. Cheng, B. Ren, *J. Phys. Chem. Lett*. **2019**, *10*, 2306, https://doi.org/10.1021/acs.jpclett.9b00203.
[26] Z.-F. Cai, J. P. Merino, W. Fang, N. Kumar, J. O. Richardson, S. De Feyter, R. Zenobi, *J. Am. Chem. Soc*. **2022**, *144*, 538, https://doi.org/10.1021/jacs.1c11263.
[27] Z. Chen, S. Jiang, G. Kang, D. Nguyen, G. C. Schatz, R. P. Van Duyne, *J. Am. Chem. Soc*. **2019**, *141*, 15684, https://doi.org/10.1021/jacs.9b07979.
[28] R. Wang, J. Li, J. Rigor, N. Large, P. Z. El-Khoury, A. Yu. Rogachev, D. Kurouski, *J. Phys. Chem. C* **2020**, *124*, 2238, https://doi.org/10.1021/acs.jpcc.9b12002.
[29] A. Bhattarai, P. Z. El-Khoury, *J. Phys. Chem. Lett*. **2019**, *10*, 2817, https://doi.org/10.1021/acs.jpclett.9b00935.
[30] S. Bienz, S. H. van Vreeswijk, Y. Pandey, G. Luca Bartolomeo, B. M. Weckhuysen, R. Zenobi, N. Kumar, *Catal. Sci. Technol.* **2022**, *12*, 5795, https://doi.org/10.1039/D2CY01348G.
[31] J. H. K. Pfisterer, M. Baghernejad, G. Giuzio, K. F. Domke, *Nat. Commun*. **2019**, *10*, 5702, https://doi.org/10.1038/s41467-019-13692-3.
[32] H.-S. Su, H.-S. Feng, Q.-Q. Zhao, X.-G. Zhang, J.-J. Sun, Y. He, S.-C. Huang, T.-X. Huang, J.-H. Zhong, D.-Y. Wu, B. Ren, *J. Am. Chem. Soc*. **2020**, *142*, 1341, https://doi.org/10.1021/jacs.9b10512.
[33] Z.-F. Cai, Z.-X. Tang, Y. Zhang, N. Kumar, *Angew Chem. Int. Ed*. **2024**, *63*, e202318682, https://doi.org/10.1002/anie.202318682.
[34] Z. Zhang, M. Richard-Lacroix, V. Deckert, *Faraday Discuss.* **2017**, *205*, 213, https://doi.org/10.1039/C7FD00157F.
[35] F. Shao, W. Wang, W. Yang, Z. Yang, Y. Zhang, J. Lan, A. Dieter Schlüter, R. Zenobi, *Nat. Commun*. **2021**, *12*, 4557, https://doi.org/10.1038/s41467-021-24856-5.
[36] X. Wang, D. Zhang, K. Braun, H.-J. Egelhaaf, C. J. Brabec, A. J. Meixner, *Adv. Funct. Mater.* **2010**, *20*, 492, https://doi.org/10.1002/adfm.200901930.
[37] N. Kumar, A. Zoladek-Lemanczyk, A. A. Y. Guilbert, W. Su, S. M. Tuladhar, T. Kirchartz, B. C. Schroeder, I. McCulloch, J. Nelson, D. Roy, F. A. Castro, *Nanoscale* **2017**, *9*, 2723, https://doi.org/10.1039/C6NR09057E.
[38] S. Bienz, G. Spaggiari, D. Calestani, G. Trevisi, D. Bersani, R. Zenobi, N. Kumar, *ACS Appl. Mater. Interfaces* **2024**, *16*, 14704, https://doi.org/10.1021/acsami.3c17115.
[39] E. Rodriguez-Boulan, G. Kreitzer, A. Müsch, *Nat. Rev. Mol. Cell Biol*. **2005**, *6*, 233, https://doi.org/10.1038/nrm1593.
[40] B. N. Manz, J. T. Groves, *Nat. Rev. Mol. Cell Biol*. **2010**, *11*, 342, https://doi.org/10.1038/nrm2883.
[41] J. N. Israelachvili, S. Marčelja, R. G. Horn, *Q. Rev. Biophys*. **1980**, *13*, 121, https://doi.org/10.1017/S0033583500001645.
[42] A. Luchini, G. Vitiello, *Biomimetics* **2021**, *6*, 3, https://doi.org/10.3390/biomimetics6010003.
[43] S. Bonhommeau, G. S. Cooney, Y. Huang, *Chem. Soc. Rev*. **2022**, *51*, 2416, https://doi.org/10.1039/D1CS01039E.
[44] Y. Pandey, A. Ingold, N. Kumar, R. Zenobi, *Nanoscale* **2024**, *16*, 10578, https://doi.org/10.1039/D4NR00816B.
[45] L. Opilik, T. Bauer, T. Schmid, J. Stadler, R. Zenobi, *Phys. Chem. Chem. Phys*. **2011**, *13*, 9978, https://doi.org/10.1039/C0CP02832K.
[46] Y. Pandey, N. Kumar, G. Goubert, R. Zenobi, *Angew. Chem. Int. Ed.* **2021**, *60*, 19041, https://doi.org/10.1002/anie.202106128.
[47] D. Mrđenović, W. Ge, N. Kumar, R. Zenobi, *Angew. Chem. Int. Ed.* **2022**, *134*, e202210288, https://doi.org/10.1002/ange.202210288.
[48] C. Xu, T. Käser, Y. Xia, N. Kumar, R. Zenobi, *J. Phys. Chem. Lett*. **2024**, *15*, 10237, https://doi.org/10.1021/acs.jpclett.4c01994.
[49] T. Stepanenko, K. Sofińska, N. Wilkosz, J. Dybas, E. Wiercigroch, K. Bulat, E. Szczesny-Malysiak, K. Skirlińska-Nosek, S. Seweryn, J. Chwiej, E. Lipiec, K. M. Marzec, *Analyst* **2024**, *149*, 778, https://doi.org/10.1039/D3AN01658G.
[50] D. Mrđenović, Z.-X. Tang, Y. Pandey, W. Su, Y. Zhang, N. Kumar, R. Zenobi, *Nano Lett*. **2023**, *23*, 3939, https://doi.org/10.1021/acs.nanolett.3c00689.
[51] J. Lombard, *Biol. Direct* **2014**, *9*, 32, https://doi.org/10.1186/s13062-014-0032-7.
[52] N. Kumar, M. M. Drozdz, H. Jiang, D. M. Santos, D. J. Vaux, *Chem. Commun*. **2017**, *53*, 2451, https://doi.org/10.1039/C6CC10226C.
[53] K. D. Alexander, Z. D. Schultz, *Anal. Chem*. **2012**, *84*, 7408, https://doi.org/10.1021/ac301739k.
[54] M. B. Stone, S. A. Shelby, S. L. Veatch, *Chem. Rev*. **2017**, *117*, 7457, https://doi.org/10.1021/acs.chemrev.6b00716.
[55] R. Böhme, M. Richter, D. Cialla, P. Rösch, V. Deckert, J. Popp, *J. Raman Spectrosc.* **2009**, *40*, 1452, https://doi.org/10.1002/jrs.2433.
[56] M. Richter, M. Hedegaard, T. Deckert-Gaudig, P. Lampen, V. Deckert, *Small* **2011**, *7*, 209, https://doi.org/10.1002/smll.201001503.
[57] J. V. Barth, G. Costantini, K. Kern, *Nature* **2005**, *437*, 671, https://doi.org/10.1038/nature04166.
[58] L. Grill, M. Dyer, L. Lafferentz, M. Persson, M. V. Peters, S. Hecht, *Nat. Nanotechnol*. **2007**, *2*, 687, https://doi.org/10.1038/nnano.2007.346.
[59] S. Mahapatra, J. F. Schultz, L. Li, X. Zhang, N. Jiang, *J. Am. Chem. Soc.* **2022**, *144*, 2051, https://doi.org/10.1021/jacs.1c11547.
[60] L. Verstraete, J. Greenwood, B. E. Hirsch, S. De Feyter, *ACS Nano* **2016**, *10*, 10706, https://doi.org/10.1021/acsnano.6b05954.
[61] K. Anggara, L. Sršan, T. Jaroentomeechai, X. Wu, S. Rauschenbach, Y. Narimatsu, H. Clausen, T. Ziegler, R. L. Miller, K. Kern, *Science* **2023**, *382*, 219, https://doi.org/10.1126/science.adh3856.
[62] L. Yu, Y. Xia, T. Hu, B. Daelemans, F. S. De, *CCS Chem*. **2024**, *6*, 1024, https://doi.org/10.31635/ccschem.024.202303614.
[63] Y. Xia, J. Seibel, S. De Feyter, *Aggregate* **2022**, *3*, e205, https://doi.org/10.1002/agt2.205.
[64] S. Jiang, Y. Zhang, R. Zhang, C. Hu, M. Liao, Y. Luo, J. Yang, Z. Dong, J. G. Hou, *Nat. Nanotechnol*. **2015**, *10*, 865, https://doi.org/10.1038/nnano.2015.170.
[65] Z.-F. Cai, L.-Q. Zheng, Y. Zhang, R. Zenobi, *J. Am. Chem. Soc*. **2021**, *143*, 12380, https://doi.org/10.1021/jacs.1c06366.
[66] Z.-F. Cai, T. Käser, N. Kumar, R. Zenobi, *J. Phys. Chem. Lett*. **2022**, *13*, 4864, https://doi.org/10.1021/acs.jpclett.2c01112.

License and Terms

The definitive version of this article is the electronic one that can be found at https://doi.org/10.2533/chimia.2025.52